ACS Macro Letters

Letter

pubs.acs.org/macroletters

Rearrangement of Nanoporous Cavity Structures in Crystalline Syndiotactic Polystyrene Associated with Stress-Induced Phase Transition

Yoshinori Tamai*

Department of Applied Physics, Graduate School of Engineering, University of Fukui, 3-9-1 Bunkyo, Fukui 910-8507, Japan

ABSTRACT: This work demonstrates the possibility of rearranging nanoporous cavity structures in crystalline syndiotactic polystyrene (s-PS) by applying external stresses. A molecular dynamics (MD) simulation was performed for the s-PS crystal with increasing or decreasing of each stress tensor component, starting from the nanoporous ε form. Upon uniaxial compression along the *b*-axis, the ε form was transformed into a lower density porous form, accompanied by significant elongation of the *a*-axis. The new form, named the S−I form, was stable only under the stress and was transformed into the γ form after release of the stress. The cavity structure was drastically changed by the transition. The straight cylindrical channels in the ε form, which may be used for the separation of organic solvents, were rearranged to narrower zigzag channels in the S−I form, which is suitable for the precise separation of gases. The molecular cavities disappeared after release of the stress, associated with the transition to the γ form.

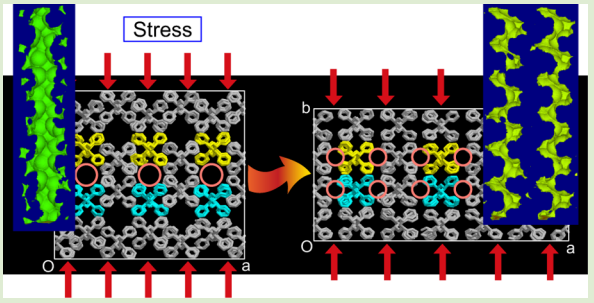

Syndiotactic polystyrene (s-PS) is known for its unusual crystal polymorphism.[1−3] There are five main polymorphs of s-PS: α, β, γ, δ, and ε forms. The main-chain conformation of the α and β forms is *trans* planar (TTTT), while that of the γ, δ, and ε forms is s(2/1)2 helical (TTGG). The α and β forms are obtained by melt processing and the other forms by solution processing. The δ form, a clathrate compound (cocrystal) with solvent, is obtained by crystallization under the presence of an organic solvent.[4] Removal of the encaged solvent molecules from the δ form produces the emptied δ_e form,[5] in which subnanoscale molecular cavities[6] are created by release of the guest molecules. These cavities disappear upon thermal treatment above 400 K, which produces the high density γ form.[7] The nanoporous ε form, in which cylindrical channels exist along the *c*-axis, has recently been obtained by treatment of the γ form with liquid chloroform.[8,9]

Because of their nanoporous or subnanoscale cavity structures, it is highly expected that s-PS crystals will be useful as molecular separation or storage materials.[2,4] For these applications, it is very important to control the size, shape, and connectivity of the cavities in the crystals in connection with sorption and diffusion behavior of small molecules. Several molecular simulation studies have been performed to clarify these relations, for example, cavity structures,[10−12] diffusion of gases,[11,13,14] reorientational motion of guest solvents,[15] and sorption of small molecules.[11,16−18] The results suggest the possibility of controlling the sorption and permeation behavior of small molecules in the crystals using external stimuli such as temperature, pressure, and stress through changes in cavity structure.

The control of crystal structure using external stimulus is encouraged by several experimental and theoretical studies. For example, a thermally induced phase transition from the δ_e to the γ form was investigated in detail both experimentally[19] and by our previous simulation.[20] A strain-induced conformational transition from TTGG (γ) to TTTT (α) has also been reported.[21] By annealing under high pressure, the higher density β form is obtained rather than the lower density α form.[22] In contrast, the transition from β to α form was observed at well below the melting temperature with mechanical tensile deformation.[23] It is important to establish the relationships between cavity structure and external stimulus.

Here I report a rearrangement of nanoporous cavity structures in s-PS crystal associated with a crystal phase transition induced by external uniaxial stresses, using a molecular dynamics (MD) simulation. Starting from the ε form, the crystal was exposed to the stress, and each component of the stress tensor was increased or decreased separately. A drastic phase transition from the ε form to a new porous crystalline form, which is stable under the uniaxial compressive stress along the *b*-axis, was found.

The energy-minimized structure of the ε form was equilibrated by a 55 ps MD simulation, followed by sampling runs of 200 ps at 300 K. The γ form, the initial structure of which is obtained from a previous study,[20] and the δ_e form were also simulated using the same procedure for comparison. The crystal cell dimensions and density under atmospheric pressure

Received: July 24, 2013
Accepted: September 3, 2013
Published: September 5, 2013

   dx.doi.org/10.1021/mz400386z | *ACS Macro Lett.* 2013, 2, 834−838

obtained from the present simulation are listed in Table 1 compared with those of experiments. The experimental values

Table 1. Crystal Cell Dimensions and Density of s-PS without Stresses

form	a (Å)	b (Å)	c (Å)	γ (deg.)	d (g/cm^3)
			simulation		
ε	16.19	21.49	7.96	90.00	0.999
δ_e	17.40	11.75	7.81	114.98	0.956
γ	19.43	8.53	7.93	83.47	1.059
			experiment		
ε^a	16.1	21.8	7.9	90.00	0.98
$\delta_e{}^b$	17.4	11.85	7.70	117	0.977
γ^c	19.18	8.62			1.07

[a]Petraccone et al.[9] [b]De Rosa et al.[5] [c]Estimated from the XRD data of Wang et al.,[7] exchanging (010) and (200) reflections.[20]

are satisfactorily reproduced by the simulation. Therefore, the present model is sufficiently applicable to the s-PS crystals.

External stress was then applied to the ε form by varying each component of the symmetric tensor $\sum$ (see eqs 1 and 2 in the section Simulation Details) at 300 K. A significant phase transition was observed during the increasing process of $\sum_{yy}$ and the decreasing process of $\sum_{zz}$, which correspond to the uniaxial compression along the b-axis and the uniaxial tension along the c-axis, respectively. In the case of the other stress treatments, the crystal was significantly collapsed before reaching the upper or lower limits of the $\sum$ scans. The xx, yy, and zz components of the stress tensors at the yielding points for the uniaxial extension along the a-, b-, and c-axes were 210, 240, and 1820 MPa, respectively. The corresponding strains were 3.9, 9.5, and 10.2%, respectively. Because of the constraint by the small unit cell and the infinite connectivity of polymer chains along the c-axis, the yielding points may have been shifted upward relative to those observed in real experiments. The calculated Young's modulus along the c-axis, E_c, was 18.3 GPa. The value is reasonable compared with those determined experimentally for polymer crystals with a helical conformation, for example, 34 GPa for isotactic polypropylene (i-PP) and 11.8 GPa for i-PS.[24] The calculated Young's moduli perpendicular to the c-axis, E_a = 7.3 and E_b = 3.7 GPa, are smaller than E_c and also agree well with those determined for nonpolar polymer crystals, for example, 3.0 GPa for i-PP and 3.7 GPa for polyethylene (PE) by experiments[25] and 6.9–9.2 GPa for PE by a model calculation.[26]

Figure 1 shows the dependence of the edge length, density, and potential energy on $\sum_{yy}$. During the compression process from $\sum_{yy}$ = 0, the crystal was transformed into another form at $\sum_{yy}$ = 15 kJ/mol Å, which corresponds to a compressive stress of S_{yy} = 410 MPa. The transition started at 8.7% strain and completed within 15 ps after initiation, with relaxation of the S_{yy} value to approximately 280 MPa, accompanied by the elongation of the a-axis. This transition is apparently very strange because the density significantly decreases, from 1.058 to 0.967 g/cm^3, upon compression along the b-axis. This decrease in density was caused by significant elongation of the a-axis. Upon further compression, the crystal was transformed into a higher density structure at $\sum_{yy}$ = 36 kJ/mol Å (S_{yy} = 540 MPa). A hysteresis-like behavior was observed during the stress release process from $\sum_{yy}$ = 25 kJ/mol Å; the low-density structure was preserved even below $\sum_{yy}$ = 15 kJ/mol Å. This low-density crystal is named here as the S–I form. The crystal

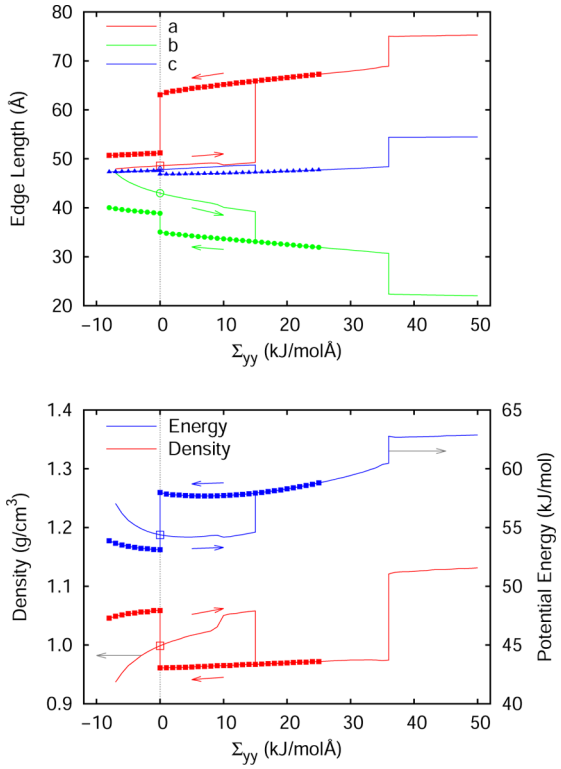

Figure 1. Change in MD unit cell edge length, density, and potential energy per monomer unit upon uniaxial stress along the y-axis. The simulation was started from $\sum_{yy}$ = 0 (open symbol). The solid lines without symbols show the sweep process from $\sum_{yy}$ = 0, and those with solid symbols show the reverse sweep from $\sum_{yy}$ = 25 kJ/mol Å.

then transformed into a higher density structure at $\sum_{yy}$ = 0, temporarily called the γ' form (this form was found to be identical to the γ form as discussed below). The S–I form was stable only under stress along the b-axis. In the case of the $\sum_{zz}$ scan, the crystal was transformed into an all-trans crystal similar to the β form with some defects at $\sum_{zz}$ = −40 kJ/mol Å (S_{zz} = −1820 MPa). Table 2 lists the crystal cell dimensions and density of the S–I form at $\sum_{yy}$ = 10 kJ/mol Å (S_{yy} = 180 MPa) and those of the γ' form. These structures were used for later analysis.

Table 2. Crystal Cell Dimensions and Density of s-PS after Phase Transition by Simulation of Loading and Release of Stress along the b-Axis

form	a (Å)	b (Å)	c (Å)	γ (deg.)	d (g/cm^3)
S–I[a]	21.73	16.83	7.84	90.01	0.965
$\gamma'{}^b$	17.07	19.43	7.93	83.46	1.059
$\gamma'{}^c$	19.43	8.54	7.93	83.46	1.059

[a]Under the stress of S_{yy} = 180 MPa ($\sum_{yy}$ = 10 kJ/molÅ). [b]After stress release, in the same crystal unit as that of the ε form. [c]After stress release, in the same crystal unit as that of the γ form; i.e., the a- and b-axes are switched, and the value of b is divided by 2.

Figure 2 shows snapshots of the ε, S–I, and γ' forms projected on the a–b plane. The helical axis of the s-PS chain is parallel to the c-axis. In the ε form (Figure 2a), cylindrical channels exist along the c-axis, shown by circles as examples. The crystal was transformed into the S–I form (Figure 2b) after the uniaxial stress treatment. During this transition the colored chains in Figure 2a moved into the cylindrical pore and

dx.doi.org/10.1021/mz400386z | ACS Macro Lett. 2013, 2, 834–838

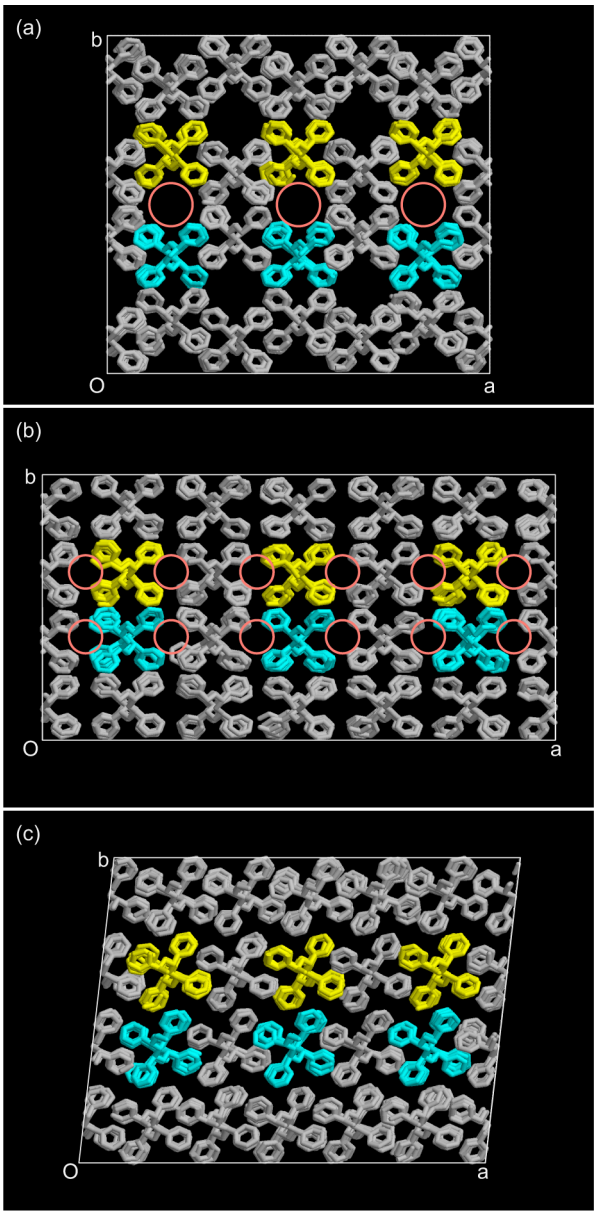

Figure 2. Snapshots of s-PS crystals: (a) ε form, (b) S−I form (at $\sum_{yy}$ = 10 kJ/molÅ), and (c) γ' form. Parts of the chains are colored to guide the eye. The orange circles show the positions of channels along the *c*-axis. The γ' form is identical to the γ form as discussed in the text.

spread out the space between pairs of chains along the *a*-axis. Therefore, the elongation of the *a*-axis is necessary for the transition. Each cylindrical channel in the ε form was divided into two portions, as shown by the circles in Figure 2b. The porous nature of the crystal is preserved because the density decreases to 0.965 g/cm^3, which is approximately the same as that of the empty δ_e form: 0.977 g/cm^3.[5]

After release of the uniaxial stress to atmospheric pressure, the S−I form was transformed into the higher density γ' form as shown in Figure 2c, in which the molecular cavities have disappeared. The structure is the same as that of the γ form obtained by our previous simulation.[20] The snapshot in that paper[20] can be recovered by 180° rotation around the *x*-axis followed by rotation around the *z*-axis to let the *b*-axis coincide with the *x*-axis. The converted crystal cell dimensions are shown in Table 2 (the data with note *c*). The values satisfactorily agree with the crystal cell dimensions of the γ form of the present simulation and also with the estimated *a* and *b* values obtained from the X-ray diffraction data of Wang et al.[7] Therefore, the γ' form is identical to the γ form.

The thermostability of the polymorphs was examined using a series of stepwise heating simulations at 50 K intervals. The deformation temperatures T_d were 600, 700, and 800 K for the δ_e, S−I, and ε forms, respectively. The δ_e form was transformed into the γ form, as observed in our previous study[20] (the T_d value was 50 K higher in the present simulation due to the use of the Ewald sum method to handle the Coulomb interaction). The S−I and ε forms were also transformed into the other forms. The T_d values appear high compared with the transition temperature for the δ_e to γ form transition, 370−400 K,[3] and the experimental melting temperature of s-PS, ∼550 K.[1] Because of the restriction of the unit cell, infinite connectivity of chains along the *c*-axis, and extremely short holding time at each temperature, the obtained T_d values are likely to have been overestimated. Although the absolute values of T_d may be shifted, a relative comparison between polymorphs is justified. It is concluded that the S−I form is more stable than the δ_e form and less stable than the ε form.

To confirm the reproducibility of the transition shown in Figure 1, two more simulation runs at 300 K were performed. The transition stresses were completely identical among these three runs. MD runs at higher temperatures, i.e., 350, 400, 450, and 500 K, were also performed. The transition behavior was found to be similar between all runs and at all temperatures for the $\sum_{yy}$ scan, although the transition stresses shifted to lower values, for example, $\sum_{yy}$ = 9 kJ/mol Å (S_{yy} ∼ 220 MPa) at 500 K. As for the $\sum_{zz}$ scan, the transition behavior was dependent on the temperature because it requires the conformational transition. The ε form was completely transformed into the β form with no defects at $\sum_{zz}$ = −35 kJ/mol Å (S_{zz} = −1500 MPa) at 500 K.

It is interesting that the transition to the S−I form does not require a high chain mobility (premelting); the transitions occur well below the melting temperature, and the TTGG conformation is preserved during transition. An actual solid to solid transition scheme has also been reported for the case of a transition from β to α forms caused by tensile mechanical strain at 403−491 K.[23] In the present simulation, the transition to the S−I form occurs also below the glass transition temperature T_g (∼350 K), which reflects the relaxation of the main chain. In real crystal samples, the amorphous regions amount to 20−40%.[23] The crystal structural transition may be suppressed below T_g because the frozen amorphous regions act as a kind of rigid cage and prevent the conformational transition of polymer chains. In contrast, the T_g value has no critical meaning in the present simulation because the present model is an ideal single crystal with no amorphous regions and the main-chain conformation is preserved during the transition, although the transition occurs more easily at higher temperature. The present simulation clearly proves the existence of a transition path from the ε to γ forms via the intermediate S−I form without large deformation of chains.

Both the start and end point structures along the transition path from the ε to the γ form via the S−I form, i.e., the ε and γ form structures, agree well with experimental data. The response to the stress was also reasonable, considering the calculated Young's moduli. Furthermore, the structural transition behavior between known polymorphs, i.e., from the

dx.doi.org/10.1021/mz400386z | ACS Macro Lett. 2013, 2, 834−838

δ_e to γ forms and from the ε to β forms, can be simulated satisfactorily. Crystal modifications which are stable only under stress have also been reported for the other polymers; for example, poly(butylene terephthalate) (PBT),[27] poly(tetramethylene succinate) (PTMS),[28] and poly(ethylene succinate) (PES).[29] The critical stresses for PBT, PTMS, and PES, assuming the first-order phase transition, are 75, 140, and 190 MPa, respectively, at room temperature.[29] Thus, the simulated transition stresses, S_{yy} = 410−220 MPa at 300−500 K, which are generally higher than the critical stress, are in an acceptable range. The transition path via the S−I form is therefore sufficiently realistic. Considering the thermostability in the heating simulation, the S−I form should exist stably under real conditions, though direct experimental observation of the S−I form has not yet been reported at this time. Because the ε form can be obtained from the γ form by a solvent treatment,[8,9] the transition path of $\gamma \rightarrow \varepsilon \rightarrow$ S−I $\rightarrow \gamma$ is recyclable. This also supports the existence of the S−I form.

A free volume analysis was performed using the same procedure as that in our previous studies.[11,12,30] An MD unit cell was divided into grid points of 0.2 Å intervals. The accessible grid points, where a probe of radius 0.7 Å can be settled without overlapping any other polymer atoms, are shown in Figure 3. Only three or six continuous clusters are shown for the ε form (Figure 3a) and the S−I form (Figure 3b), respectively, for clarity. The cavity structure is drastically changed by the stress treatment. In the ε form, the cylindrical channels are wide and straight. The fraction of accessible grid points along the *c*-axis is 1.0 around the center axis of each channel, as indicated by the color scale (violet); completely empty "pipes" exist along the *c*-axis. The accessible fraction along the *c*-axis is at most 0.4 or so (green) for the S−I form, and the channels along the *c*-axis are zigzag in shape. The free volumes in the S−I form consist of many ellipsoidal small cavities connected by narrow channels. Although each channel in the S−I form is narrower than that in the ε form, the total free volume of the S−I form is larger because its density is lower.

In a preliminary simulation on the diffusion of small gases, such as O_2, N_2, CO_2, and CH_4, in the crystals, the separation factors in the ε form are very low because the radius of capillary is too large for these gases to separate; all of the gases can permeate easily. In contrast, the narrower channels in the S−I form lead to significantly higher separation factors. Especially, the diffusion of CO_2 is surprisingly effective in the new form. The results on the permeation behavior in the crystal will be presented in an upcoming paper.

This letter has demonstrated the possibility of rearranging the nanoporous cavity structures in s-PS crystals by applying external stresses. Upon uniaxial compression along the *b*-axis, the nanoporous ε form was transformed into a lower-density porous form (named S−I form), accompanied by significant elongation of the *a*-axis. After release of the stress, the S−I form was transformed into the γ form, and the molecular cavities disappeared. Melting or large deformation of chain conformation is not required for these transitions; the TTGG helix conformation is preserved. The significance of the S−I form resides in its remarkable cavity structure, which was drastically changed through the crystal structural transition. The straight cylindrical channels in the ε form, which may be used for the separation of organic solvents, can be modified to narrower zigzag channels which are suitable for the precise separation of gases such as CO_2, by applying external stress.

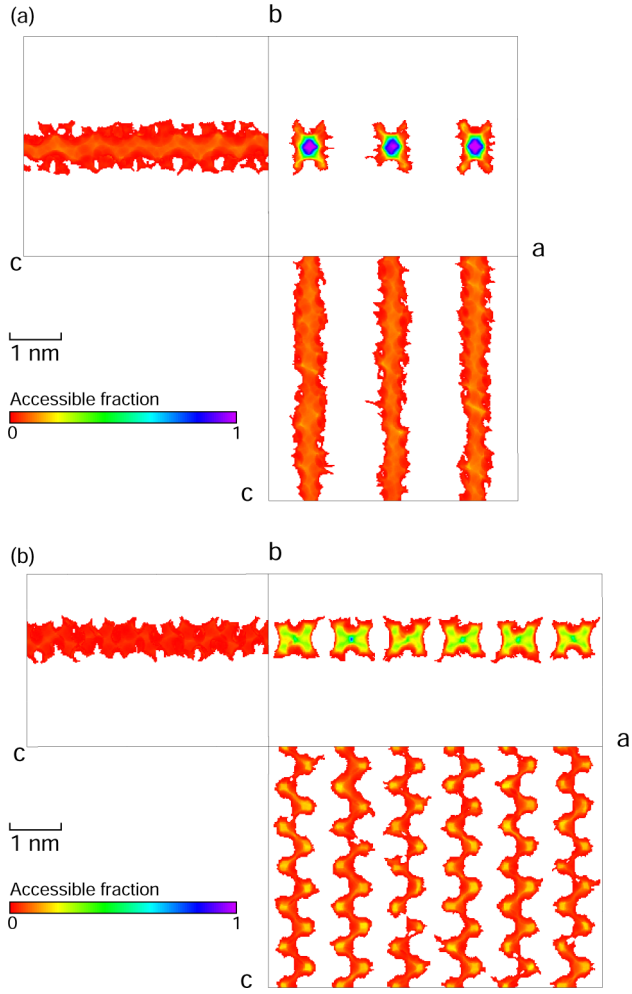

Figure 3. Projections of accessible volume clusters in s-PS crystals calculated for a probe of radius 0.7 Å. (a) ε form, the three columns correspond to cavities in Figure 2a (orange circles). (b) S−I form, the six columns correspond to cavities in Figure 2b (upper row of orange circles). The color scale indicates the fraction of accessible grid points for the depth direction.

SIMULATION DETAILS

The initial structure of the ε form was generated according to the space group *Pbcn*, based on the structure determined by X-ray diffraction experiments.[8,9] For comparison, the δ_e and γ forms were also simulated. The initial structure of the δ_e form was taken from experimental data,[5] and that of the γ form was taken from our previous simulation study.[20] The space group of the latter two forms is $P2_1/a$. The crystal was modeled as a single crystal in which an infinite number of monomer units are connected along the *c*-axis by the periodic boundary condition. The MD unit cells consist of 3 × 2 × 6 crystal unit cells for the ε form and 3 × 4 × 6 cells for the other forms. A total of 24 chains (9216 atoms) are contained in each MD unit cell.

The all-atom force field AMBER[31] was used. The partial charges were assigned only for aromatic hydrogen (+0.085*e*) and aromatic carbon bonded to the hydrogen (−0.085*e*).[32] The model was used in our previous studies[11,12,14,15,20] and found that densities and crystal cell dimensions of α, β, δ, and δ_e forms were satisfactorily reproduced. The model was also applied for CO_2 sorption in the δ_e form by other authors,[18] and the sorption isotherms were successfully reproduced. Therefore, the application of the present model to the simulation of s-PS crystals is justified. Bond lengths were constrained by the SHAKE method.[33] Lennard-Jones interactions were smoothly cut off at 9 Å with the long-range correction. Long-range Coulomb interactions were considered for infinite distance using the Ewald sum method.

dx.doi.org/10.1021/mz400386z | *ACS Macro Lett.* 2013, 2, 834−838

The pressure tensor was controlled by the Parrinello–Rahman[34] method. Under external stress **S** and hydrostatic pressure p, the equation of motion for the cell matrix **h**, whose columns are the components of edge vectors **a**, **b**, and **c**, is expressed as

$$W\ddot{\mathbf{h}} = (\boldsymbol{\pi} - p)\boldsymbol{\sigma} - \mathbf{h}\sum \quad (1)$$

where W is the virtual mass; $\boldsymbol{\sigma} \equiv V(\mathbf{h}^{-1})^t$ is a matrix (V is the volume of a unit cell); $\boldsymbol{\pi}$ is the instantaneous pressure tensor; and the symmetric tensor $\sum$ is related to **S** as

$$\sum = \mathbf{h}_0^{-1}(\mathbf{S} - p)(\mathbf{h}_0^{-1})^t V_0 \quad (2)$$

where the subscript 0 denotes the reference state.[34] In the present study, the equations of motion were modified to combine with the Nosé[35] method for the temperature control. The equations of motion were solved by a variant of the Verlet algorithm[36,37] with a time step of 1 fs.

The external stresses were applied to the crystals by varying each component of the symmetric tensor $\sum$ in the range −50 to 50 kJ/mol Å under constant hydrostatic pressure of p = 0.1 MPa. The components of $\sum$ were stepwise increased or decreased by 1 kJ/mol Å with equilibration runs of 30 ps and sampling runs of 100 ps at each $\sum$. A stepwise heating simulation was also performed to estimate the thermostability of the crystals. The temperature was increased by intervals of 50 K with 130 ps runs at each temperature within the range 300–1000 K. All simulation runs were performed by the molecular simulation program PAMPS[38] coded by the author.

AUTHOR INFORMATION

Corresponding Author

*E-mail: tamai@polymer.apphy.u-fukui.ac.jp.

Notes

The authors declare no competing financial interest.

ACKNOWLEDGMENTS

This work was partly supported by MEXT/JSPS KAKENHI, Grant-in-Aid for Scientific Research (C), 19550121. The numerical calculations were carried out on System A/B at the Institute for Information Management and Communication, Kyoto University. The costs of these systems were supported by Center for Information Initiative, University of Fukui.

REFERENCES

(1) Guerra, G.; Vitagliano, V. M.; De Rosa, C.; Petraccone, V.; Corradini, P. *Macromolecules* **1990**, *23*, 1539–1544.
(2) Milano, G.; Guerra, G. *Prog. Mater. Sci.* **2009**, *54*, 68–88.
(3) Gowd, E. B.; Tashiro, K.; Ramesh, C. *Prog. Polym. Sci.* **2009**, *34*, 280–315.
(4) Guerra, G.; Daniel, C.; Rizzo, P.; Tarallo, O. *J. Polym. Sci., Part B: Polym. Phys.* **2012**, *50*, 305–322.
(5) De Rosa, C.; Guerra, G.; Petraccone, V.; Pirozzi, B. *Macromolecules* **1997**, *30*, 4147–4152.
(6) Tsujita, Y.; Yoshimizu, H.; Okamoto, S. *J. Mol. Struct.* **2005**, *739*, 3–12.
(7) Wang, Y. K.; Savage, J. D.; Yang, D.; Hsu, S. L. *Macromolecules* **1992**, *25*, 3659–3666.
(8) Rizzo, P.; Daniel, C.; De Girolamo Del Mauro, A.; Guerra, G. *Chem. Mater.* **2007**, *19*, 3864–3866.
(9) Petraccone, V.; Ruiz de Ballesteros, O.; Tarallo, O.; Rizzo, P.; Guerra, G. *Chem. Mater.* **2008**, *20*, 3663–3668.
(10) Milano, G.; Venditto, V.; Guerra, G.; Cavallo, L.; Ciambelli, P.; Sannino, D. *Chem. Mater.* **2001**, *13*, 1506–1511.
(11) Tamai, Y.; Fukuda, M. *Polymer* **2003**, *44*, 3279–3289.
(12) Tamai, Y.; Fukuda, M. *J. Chem. Phys.* **2004**, *121*, 12085–12093.
(13) Milano, G.; Guerra, G.; Müller-Plathe, F. *Chem. Mater.* **2002**, *14*, 2977–2982.
(14) Tamai, Y.; Fukuda, M. *Chem. Phys. Lett.* **2003**, *371*, 217–222.
(15) Tamai, Y.; Fukuda, M. *Chem. Phys. Lett.* **2003**, *371*, 620–625.
(16) Figueroa-Gerstenmaier, S.; Daniel, C.; Milano, G.; Vitillo, J. G.; Zavorotynska, O.; Spoto, G.; Guerra, G. *Macromolecules* **2010**, *43*, 8594–8601.
(17) Figueroa-Gerstenmaier, S.; Daniel, C.; Milano, G.; Guerra, G.; Zavorotynska, O.; Vitillo, J. G.; Zecchina, A.; Spoto, G. *Phys. Chem. Chem. Phys.* **2010**, *12*, 5369–5374.
(18) Sanguigno, L.; Cosentino, F.; Larobina, D.; Mensitieri, G. *Soft Mater.* **2011**, *9*, 169–182.
(19) Gowd, E. B.; Shibayama, N.; Tashiro, K. *Macromolecules* **2006**, *39*, 8412–8418.
(20) Tamai, Y.; Fukuda, M. *Macromol. Rapid Commun.* **2002**, *23*, 891–895.
(21) De Candia, F.; Russo, R.; Vittoria, V. *Polym. Commun.* **1991**, *32*, 306–309.
(22) Sun, Z.; Morgan, R. J.; Lewis, D. N. *Polymer* **1992**, *33*, 660–661.
(23) Ouchi, T.; Nagasaka, S.; Hotta, A. *Macromolecules* **2011**, *44*, 2112–2119.
(24) Sakurada, I.; Kaji, K. *J. Polym. Sci., Part C: Polym. Symp.* **1970**, *31*, 57–76.
(25) Sakurada, I.; Ito, T.; Nakamae, K. *J. Polym. Sci., Part C: Polym. Symp.* **1966**, *15*, 75–91.
(26) Tashiro, K.; Kobayashi, M.; Tadokoro, H. *Macromolecules* **1978**, *11*, 914–918.
(27) Tashiro, K.; Nakai, Y.; Kobayashi, M.; Tadokoro, H. *Macromolecules* **1980**, *13*, 137–145.
(28) Ichikawa, Y.; Suzuki, J.; Washiyama, J.; Moteki, Y.; Noguchi, K.; Okuyama, K. *Polymer* **1994**, *35*, 3338–3339.
(29) Ichikawa, Y.; Noguchi, K.; Okuyama, K.; Washiyama, J. *Polymer* **2001**, *42*, 3703–3708.
(30) Tamai, Y.; Tanaka, H.; Nakanishi, K. *Macromolecules* **1995**, *28*, 2544–2554.
(31) Cornell, W. D.; Cieplak, P.; Bayly, C. I.; Gould, I. R.; Merz, K. M.; Ferguson, D. M.; Spellmeyer, D. C.; Fox, T.; Caldwell, J. W.; Kollman, P. A. *J. Am. Chem. Soc.* **1995**, *117*, 5179–5197.
(32) Smith, G. D.; Ayyagari, C.; Jaffe, R. L.; Pekny, M.; Bernarbo, A. *J. Phys. Chem. A* **1998**, *102*, 4694–4702.
(33) Ryckaert, J.-P.; Ciccotti, G.; Berendsen, H. J. C. *J. Comput. Phys.* **1977**, *23*, 327–341.
(34) Parrinello, M.; Rahman, A. *J. Appl. Phys.* **1981**, *52*, 7182–7190.
(35) Nosé, S. *J. Chem. Phys.* **1984**, *81*, 511–519.
(36) Verlet, L. *Phys. Rev.* **1967**, *159*, 98–103.
(37) Ferrario, M.; Ryckaert, J. *Mol. Phys.* **1985**, *54*, 587–603.
(38) Tamai, Y.; Tanaka, H.; Nakanishi, K. *Macromolecules* **1994**, *27*, 4498–4508.